

Computing and Partitioning Cloud Feedbacks Using Cloud Property Histograms. Part I: Cloud Radiative Kernels

MARK D. ZELINKA

Department of Atmospheric Sciences, University of Washington, Seattle, Washington, and Program for Climate Model Diagnosis and Intercomparison, Lawrence Livermore National Laboratory, Livermore, California

STEPHEN A. KLEIN

Program for Climate Model Diagnosis and Intercomparison, Lawrence Livermore National Laboratory, Livermore, California

DENNIS L. HARTMANN

Department of Atmospheric Sciences, University of Washington, Seattle, Washington

(Manuscript received 12 May 2011, in final form 15 November 2011)

ABSTRACT

This study proposes a novel technique for computing cloud feedbacks using histograms of cloud fraction as a joint function of cloud-top pressure (CTP) and optical depth (τ). These histograms were generated by the International Satellite Cloud Climatology Project (ISCCP) simulator that was incorporated into doubled- CO_2 simulations from 11 global climate models in the Cloud Feedback Model Intercomparison Project. The authors use a radiative transfer model to compute top of atmosphere flux sensitivities to cloud fraction perturbations in each bin of the histogram for each month and latitude. Multiplying these cloud radiative kernels with histograms of modeled cloud fraction changes at each grid point per unit of global warming produces an estimate of cloud feedback. Spatial structures and globally integrated cloud feedbacks computed in this manner agree remarkably well with the adjusted change in cloud radiative forcing. The global and annual mean model-simulated cloud feedback is dominated by contributions from medium thickness ($3.6 < \tau \leq 23$) cloud changes, but thick ($\tau > 23$) cloud changes cause the rapid transition of cloud feedback values from positive in midlatitudes to negative poleward of 50°S and 70°N . High ($\text{CTP} \leq 440$ hPa) cloud changes are the dominant contributor to longwave (LW) cloud feedback, but because their LW and shortwave (SW) impacts are in opposition, they contribute less to the net cloud feedback than do the positive contributions from low ($\text{CTP} > 680$ hPa) cloud changes. Midlevel ($440 < \text{CTP} \leq 680$ hPa) cloud changes cause positive SW cloud feedbacks that are 80% as large as those due to low clouds. Finally, high cloud changes induce wider ranges of LW and SW cloud feedbacks across models than do low clouds.

1. Introduction

Clouds are fundamentally important to the energy budget of the planet owing to their high albedo, large emissivity, and location at colder temperatures than the surface. Relative to a hypothetical cloudless but otherwise identical planet, the global and annual mean effect of clouds at the top of atmosphere (TOA) is to increase

the amount of reflected shortwave (SW) radiation by about 48 W m^{-2} and to reduce the amount of emitted longwave (LW) radiation by about 28 W m^{-2} (Allan 2011). Thus the net effect of clouds is to cool the planet by about 20 W m^{-2} .

An important unanswered question of climate science is how cloud radiative effects will change as the planet warms because of long-lived greenhouse gases. Any systematic change in clouds that accompanies warming will induce TOA radiation anomalies that feedback on (i.e., amplify or dampen) those caused by increased greenhouse gas concentrations. In all current global climate models (GCMs), cloud feedbacks are positive (Soden and Held 2006), indicating that modeled clouds

Corresponding author address: Mark D. Zelinka, Program for Climate Model Diagnosis and Intercomparison Lawrence Livermore National Laboratory 7000 East Avenue, L-103, Livermore, CA 94551.
E-mail: zelinka1@llnl.gov

change in such a way as to cool the planet less as the planet warms. However, the intermodel spread in cloud feedback is larger than for any other radiative feedback process and is the primary contributor to the large range of climate sensitivity produced by the models (e.g., Cess et al. 1990; Soden and Held 2006; Ringer et al. 2006).

Intermodel spread in cloud feedback must be reduced if the range of possible future climates simulated by models is to be narrowed. To do so, it is necessary to identify the nature of cloud changes that give rise to cloud feedbacks within models, with an eye toward identifying those aspects that are robust from those that are not robust. Only then can physical processes that are well understood, better constrained, and/or consistently modeled be distinguished from those that are not. Such an approach requires accurate methods to quantify cloud feedback that can be applied across models using the available diagnostics archived by the modeling centers.

Three primary methods have been used previously to attribute modeled cloud feedbacks to the cloud changes from which they arise. In all cases, the cloud feedback is quantified as the change in cloud radiative forcing per unit change in global mean surface air temperature, where cloud radiative forcing is defined as the difference between clear- and all-sky TOA fluxes (e.g., Charlock and Ramanathan 1985). First, Bony et al. (2004), Bony and Dufresne (2005), and Wyant et al. (2006) used 500-hPa vertical motion as a proxy for large-scale circulation to separate the response of tropical clouds to an imposed climate change into two components: a thermodynamic component due to intrinsic temperature dependence of cloud radiative properties and a dynamic component due to changes in circulation. Second, Webb et al. (2006) compared the magnitude of the change in LW cloud forcing relative to the change in SW cloud forcing at each grid point to infer which types of cloud changes could plausibly be responsible for each local value of cloud feedback. Finally, Williams and Tselioudis (2007) and Williams and Webb (2009) employed a clustering technique to define several primary cloud regimes from International Satellite Cloud Climatology Project (ISCCP) simulator output (described below) and assessed the contributions to cloud feedback from changes in the relative frequency of occurrence of each regime and from changes in the cloud radiative forcing within each regime. All of these studies found a dominant role for low clouds in driving the intermodel spread in net cloud feedback. However, two important ambiguities remain.

First, Soden et al. (2004) have demonstrated that the change in cloud forcing may not be an accurate measure of the magnitude or even the sign of the cloud feedback because it includes noncloud-induced changes in fluxes that are irrelevant for cloud feedback. [Shell et al. (2008)

and Soden et al. (2008) proposed the method discussed below to compute cloud feedbacks that accounts for and attempts to remove the effect of clear-sky changes on the change in cloud forcing.]

The second important ambiguity in these studies is that—even if clear-sky effects are accounted for—the use of such an integrated quantity as the change in radiation at the TOA does not allow for clear identification of the nature of cloud changes from which the radiative changes arise. For example, at a location in which the change in both SW and LW cloud forcing is positive (i.e., one given the *H* classification of Webb et al. (2006)), the implied cloud response is “less/thinner low and more/higher/thicker high thin cloud.” Clearly a number of plausible cloud responses can give rise to a particular combination of LW and SW cloud-forcing changes. A similarly vague finding that is common to these studies is the small role of high clouds in contributing to both the mean and intermodel spread in cloud feedback. Is this because high clouds exhibit little change, and do so similarly across models, or because there are large but compensating changes in high clouds (e.g., large upward shifts and large reductions in coverage) that occur consistently across models? Such integrated measures potentially mask competing effects of cloud changes, which may give a false indication of robustness or deemphasize the importance of a particular type of cloud change. Therefore it is preferable to devise an alternative method in which the cloud changes that cause the cloud feedback can be determined directly.

In this paper we propose a different technique for attributing the contributions of specific types of cloud changes to cloud feedback that makes use of histograms of cloud fraction partitioned by cloud top pressure (CTP) and visible optical depth (τ), along with corresponding TOA radiative flux sensitivities to cloud fraction changes. The CTP- τ histograms of cloud fraction we use are generated by the ISCCP simulator (Klein and Jakob 1999; Webb et al. 2001) that was run inline in GCMs as part of the experiments performed for the first phase of the Cloud Feedback Model Intercomparison Project (CFMIP1; McAvaney and Le Treut 2003). The simulator provides a plausible distribution of cloud-top fractions by employing the same cloud property retrieval techniques to the model atmosphere that are used by the ISCCP passive satellite sensors observing the real atmosphere (Rossow and Schiffer 1999). Because the cloud-top fractions are individually “visible” from space and are therefore individually impacting the TOA radiative fluxes, it is possible to compute a cloud radiative kernel that describes the TOA flux sensitivity to cloud-top fraction changes in the histogram. We note that the simulator is essential as our technique cannot be applied

TABLE 1. Global climate models used in this study that took part in the Cloud Feedback Model Intercomparison Project, phase 1. Asterisks denote models for which profiles of atmospheric temperature and specific humidity were not provided. The MPI ECHAM5 model was excluded from all calculations because of incorrect implementation of the ISCCP simulator (see appendix A).

No.	Abbreviation	Modeling center	Country
1	HadSM4	Hadley Centre for Climate Prediction and Research/Met Office	United Kingdom
2	HadSM3	Hadley Centre for Climate Prediction and Research/Met Office	United Kingdom
3	HadGSM1	Hadley Centre for Climate Prediction and Research/Met Office	United Kingdom
4	UIUC	University of Illinois at Urbana–Champaign	United States
5	MIROC(lowres)	Center for Climate System Research (The University of Tokyo), National Institute for Environmental Studies, and Frontier Research Center for Global Change	Japan
6	AGCM4.0	Canadian Centre for Climate Modeling and Analysis	Canada
7	BMRC1*	Bureau of Meteorology Research Centre	Australia
8	GFDL MLM2.1*	U.S. Dept. of Commerce/National Oceanic and Atmospheric Administration (NOAA)/Geophysical Fluid Dynamics Laboratory	United States
9	IPSL CM4*	Institut Pierre Simon Laplace	France
10	MIROC(hires)*	Center for Climate System Research (The University of Tokyo), National Institute for Environmental Studies, and Frontier Research Center for Global Change	Japan
11	CCSM3.0*	National Center for Atmospheric Research	United States
12	MPI ECHAM5*	Max Planck Institute for Meteorology	Germany

to conventional GCM output because of the invalidity of the assumption that TOA flux sensitivities to cloud amount perturbations in individual layers can be added linearly to compute the net TOA flux anomaly (Shell et al. 2008; Soden et al. 2008). By providing a decomposition of the full cloud field into its individual radiatively relevant components, the ISCCP simulator removes the uncertainties associated with overlap assumptions and cloud radiative properties that preclude the construction of a cloud radiative kernel from conventional GCM output.

In the first part of this paper we document the method of computing the TOA radiative impact of cloud fraction perturbations in each bin of the CTP- and τ -partitioned histogram as a function of latitude, month, and surface albedo using a radiative transfer code. We will refer to this as a cloud radiative kernel. Then, multiplying the cloud radiative kernel with the change in cloud fraction histogram per unit of global mean surface air temperature change between a control and doubled- CO_2 climate, we compute the cloud feedbacks in the CFMIP simulations. To build confidence in our method, we demonstrate that the feedback computed from ISCCP simulator output compares remarkably well with that computed by the current benchmark of adjusting the change in cloud forcing for noncloud effects (Shell et al. 2008; Soden et al. 2008), both in the global mean sense and on a point-by-point basis. The advantage of this technique over Shell et al. (2008) and Soden et al. (2008), however, is that it allows for unambiguous quantitative attribution of the cloud types that contribute to the feedback at every location across models. We do not infer the cloud responses that are consistent with the change in cloud forcing at each location but rather

compute the cloud feedback directly from the change in cloud distribution. Finally, we finish with a brief survey of results related to the partitioning of cloud feedbacks at different altitude levels and different optical depths followed by the main conclusions of this first paper.

In Part II of this work (Zelinka et al. 2012, hereafter referred to as Part II), we propose a simple method of decomposing the change in cloud fraction histogram that allows us to quantify cloud feedbacks arising from three types of cloud changes: the change in cloud amount holding the vertical and optical depth distribution fixed, the change in vertical distribution holding the optical depth distribution and total cloud amount fixed, and the change in optical depth distribution holding the vertical distribution and total cloud amount fixed. This partitioning will facilitate attribution of cloud feedbacks to specific types of processes that change clouds.

2. Data

We make use of output from slab ocean simulations performed in 12 models as part of the CFMIP1 experiments (McAvaney and Le Treut 2003) and submitted to the Coupled Model Intercomparison Project phase 3 (CMIP3) archive (Table 1). Experiments are separately run to equilibrium for a control climate with preindustrial CO_2 and a perturbed climate with doubled CO_2 . We compute monthly mean annual cycles of surface albedo, surface air temperature, clear- and all-sky LW and SW fluxes at the TOA, profiles of atmospheric specific humidity and temperature, and ISCCP simulator–produced cloud fraction histograms (described below) from the last 20 years of each run. The difference of each field’s

annual cycle between the control and doubled CO₂ runs are used in the feedback calculations. The Bureau of Meteorology Research Centre model (BMRC1), Geophysical Fluid Dynamics Laboratory Mixed Layer Model, version 2.1 (GFDL MLM2.1), L'Institut Pierre-Simon Laplace Coupled Model, version 4 (IPSL CM4), Model for Interdisciplinary Research on Climate, high-resolution version [MIROC(hires)], Max Planck Institute (MPI) ECHAM5, and the National Center for Atmospheric Research (NCAR) Community Climate System Model, version 3.0 (CCSM3.0) models did not archive specific humidity and/or temperature, making it impossible to compute cloud feedbacks from the adjusted change in cloud radiative forcing of Shell et al. (2008) and Soden et al. (2008). For the models in which it is possible to calculate the adjusted change in cloud radiative forcing, we use the values given in Fig. 1a of Webb et al. (2006) for the radiative forcing due to doubling CO₂: 3.75 W m⁻² K⁻¹ for the Met Office (UKMO) Hadley Centre Slab Model, version 4 (HadSM4), HadSM3, and the Hadley Centre Global Slab Model, version 1 (HadGSM1) models, 3.6 W m⁻² K⁻¹ for the University of Illinois, Urbana-Champaign (UIUC) model, 3.1 W m⁻² K⁻¹ for the MIROC(lowres) model, and the mean of these three values for the Canadian Centre for Climate Modelling and Analysis (CCCma) Atmospheric General Circulation Model, version 4.0 (AGCM4.0) model. The cloud masking of the CO₂ forcing is assumed to be 16%, as in Soden et al. (2008), and no forcing is assumed to be present in the SW. For comparisons with the CAM-derived (Shell et al. 2008) radiative kernels, we use the clear- and all-sky CO₂ forcing kernels to determine cloud masking of the radiative forcing.

In all of the CFMIP models, the ISCCP simulator (Klein and Jakob 1999; Webb et al. 2001) is run inline during integration. The simulator takes the algorithm used in the ISCCP cloud retrieval (Rossow and Schiffer 1999) and applies it to the model atmosphere to determine a distribution of cloud tops partitioned by CTP and τ at every sunlit grid point and time step. It takes into account the limitations and biases that exist in ISCCP retrievals of cloud properties, such as the ability to observe these distributions only in sunlit conditions, the ability to observe only the highest cloud top in the case of multilayered clouds, and the tendency for ISCCP retrievals to overestimate CTP for very thin clouds overlying thicker clouds. To estimate the total cloud fraction in each CTP and τ bin, the simulator makes use of each model's cloud overlap assumption to compute a subgrid-scale cloud distribution from which one can determine what fraction of clouds underlying higher clouds are "visible" from space. This is important because it provides a distribution of cloud tops as a function of CTP

and τ that is consistent with how clouds impact TOA radiative fluxes and with the computation of total cloud fraction in each model. Thus, the ISCCP simulator provides a distribution of "radiatively-relevant" (from a TOA perspective) cloud tops that is consistently defined across models, unlike the cloud amount diagnostics that are defined according to each model's cloud parameterization. These features are essential for computing cloud feedbacks across an ensemble of models using the technique outlined below. (Note that inconsistencies were found in the implementation of the simulator by some modeling groups; our methods of correction and rationale for excluding the MPI ECHAM5 model are described in appendix A.) We will refer to the cloud fraction as a function of CTP and τ within the histogram as C and its change under CO₂ doubling as ΔC .

While this technique is a significant advance in our ability to diagnose cloud feedbacks from models, one must acknowledge the limitations of using ISCCP simulator output to diagnose cloud feedbacks. Known limitations include the finite resolution of the ISCCP histograms (CTP bin edges at 50, 180, 310, 440, 560, 680, 800, and 1000 hPa and τ bin edges at 0, 0.3, 1.3, 3.6, 9.4, 23, 60, and 380), the lack of diagnosis of cloud property changes from the dark half of the planet which might affect the LW cloud feedback, and the fact that the reported cloud changes may be due to clouds at significantly lower levels than the reported cloud-top pressure of the highest cloud in the column. These limitations can be expected to play some role in our ability to partition cloud feedback by cloud types; however, they are not likely to substantially negate the value of these calculations nor the fact that the ISCCP simulator remains the only credible way to quantify feedbacks from cloud property changes in the CFMIP1 archive.

3. Computation of cloud radiative kernels

To quantify the role of changes in histogram-partitioned cloud fraction (ΔC) on the TOA radiative fluxes, we first compute the overcast-sky cloud radiative forcing corresponding to each bin of the histogram in a manner similar to that described in Hartmann et al. (2001) and Kubar et al. (2007). "Overcast" refers to the fact that the cloud forcing is calculated assuming a single cloud covers 100% of the area of the column in the radiation code. We use zonal and monthly mean annual cycles of temperature and water vapor profiles computed from the last two decades of the control runs of models 1–6 (the only models for which these fields were available) averaged together as input to the Fu–Liou radiation code (Fu and Liou 1992). Our results are very insensitive to whether the model-mean or any single model's

temperature and humidity fields are used as input to the radiation code, as quantified in appendix B. We assume a spatially invariant surface emissivity of 0.99, uniform CO₂, CH₄, and N₂O mixing ratios of 330, 1.6, and 0.28 ppmv, respectively, a standard profile of ozone mixing ratio, and a solar constant of 1366 W m⁻². Calculations are performed over a range of surface albedos and solar zenith angles, as described below.

The first step in computing an overcast-sky cloud forcing matrix for any given latitude and month is to calculate clear-sky TOA LW and SW fluxes using the Fu–Liou code. “Clear sky” simply means we set liquid water content and ice water content to zero throughout the column in the radiative transfer model. Then, at that same latitude and month, the Fu–Liou code is run repeatedly, each time placing a synthetic cloud in the column with a specified CTP and τ (discussed in greater detail below). For each CTP– τ bin, TOA fluxes are computed separately for four synthetic clouds located at each corner of the bin. These four TOA fluxes are averaged together to compute one TOA flux value for each bin, and then subtracted from the clear-sky flux to compute the overcast-sky cloud forcing matrix representing the impact of each cloud type on the TOA radiative fluxes relative to clear skies. Sensitivity of our cloud feedback estimates to the assumed representative cloud properties of a given bin are quantified in appendix B.

Single-layer clouds are inserted into the atmospheric column of the radiative transfer model by setting liquid or ice water content to nonzero values at the level closest to the specified CTP. Clouds with tops warmer than 263 K are assumed to be liquid, with a liquid water content in the cloud layer equal to the liquid water path divided by the layer’s geometric thickness. We compute the liquid water path using τ and Eq. (1) of Slingo (1989) assuming an effective radius of 10 μm . For clouds with tops colder than 263 K, we compute ice water content using the parameterization of optical depth per unit of cloud geometric thickness given in Eq. (3.9a) of Fu (1996). The generalized effective ice crystal size used in this computation is determined using Eq. (3.12) of Fu (1996) with an assumed effective radius of 30 μm .

To accurately capture the diurnal range of incident solar radiation, SW TOA fluxes with and without clouds are computed for the zenith angles for each of the 24 hours of a day and then averaged before being differenced. We use the 24 zenith angles appropriate for each month and latitude, using a day in the middle of each month. Though our use of zonal mean profiles of temperature and humidity does not allow us to take into account any longitude dependence that may impact TOA fluxes, we do account for spatial differences in surface albedo by performing every calculation three times, at

surface albedos of 0.0, 0.5, and 1.0. This is necessary because the sensitivity of SW fluxes to changes in cloud fraction depends strongly on underlying albedo (e.g., an increase in cloud fraction over a dark surface will increase the SW radiation reflected from that grid point more than will the same increase over a bright surface). In sum, we generate a matrix of LW and SW overcast-sky cloud forcings for every latitude and month, and for three values of surface albedo.

Because the computation of cloud forcing for each bin of the histogram is performed using a single atmospheric column with only that cloud type present, the value in each element of the matrix is the overcast-sky cloud forcing. Dividing this matrix by 100 expresses the values in units of W m⁻² %⁻¹. This computed cloud radiative kernel (K) gives the sensitivity of TOA fluxes (R) to perturbations in cloud fraction as functions of CTP and τ .

$$K \equiv \frac{\partial R}{\partial C}. \quad (1)$$

As in the case of the standard temperature and water vapor radiative kernels of Shell et al. (2008) and Soden et al. (2008), the cloud radiative kernel depends on latitude and month. It is slightly different in that we did not compute a kernel for each longitude but we did compute a separate kernel for each of three values of surface albedo. Additionally, whereas Shell et al. (2008) and Soden et al. (2008) called the GFDL, CAM, and BMRC models’ radiation codes 8 times daily at every location on the planet for each perturbation level and feedback variable for a 1-yr simulation, we input climatological zonal and monthly mean thermodynamic profiles averaged across six models into the Fu–Liou code.

Before using the cloud radiative kernels to compute cloud feedback, they are mapped by linear interpolation from their native latitude–albedo space to latitude–longitude space using the clear-sky surface albedo at each location and month in each model’s control climate. Note that this feature of the kernel technique implies that some of the intermodel spread in SW cloud feedback will arise simply from differences in control climate clear-sky surface albedo across models, but we find that this is a small effect (see appendix B).

In Fig. 1, we show the global and annual mean cloud radiative kernels. The LW cloud radiative kernel is positive for all cloud types, indicating that increases in cloud fraction result in decreases in outgoing longwave radiation (OLR), and vice versa. The magnitude of the kernel is sensitive to both τ and CTP. For thin clouds ($\tau < 3.6$), OLR is sensitive to changes in both their optical depth and their vertical distribution, but for clouds with $\tau > 3.6$, the sensitivity of OLR to changes in the optical depth distribution becomes saturated and OLR is solely

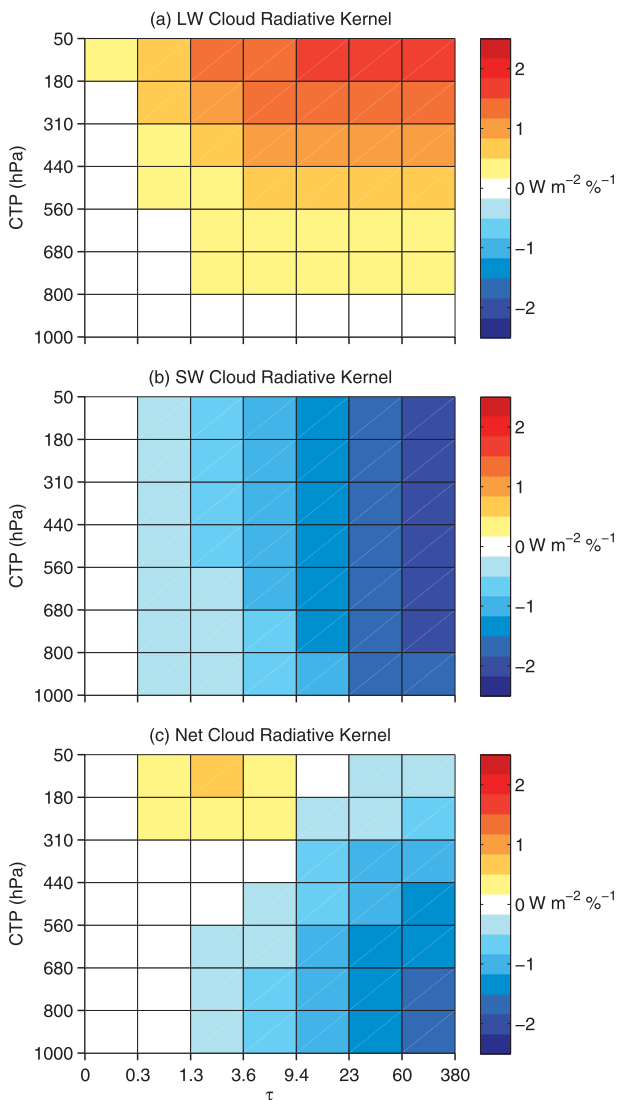


FIG. 1. Global, annual, and ensemble mean (a) LW, (b) SW, and (c) net cloud radiative kernels. In each model, the kernels have been mapped to the control climate's clear-sky surface albedo distribution before averaging in space; thus, the average kernels are weighted by the actual global distribution of clear-sky surface albedo in each model.

impacted by changes in the vertical distribution. Conversely, the SW cloud radiative kernel is negative for all cloud types, indicating that increases in cloud fraction result in increases in SW reflection to space and vice versa. The impact of cloud fraction changes on SW fluxes is much greater for thick clouds but does not depend strongly on CTP. The small dependence on CTP exhibited in the SW cloud radiative kernels is most likely due to the decreasing attenuation of SW radiation by above-cloud gaseous absorption with decreasing CTP.

Generally, a shift in the cloud distribution toward higher and thinner categories results in a positive

(warming) impact on net TOA fluxes. However, note that the largest positive net flux sensitivity is for increases in high cloud fraction for τ between 1.3 and 3.6 (see also Fig. 13b of Ackerman et al. 1988). A shift in the distribution toward lower and thicker clouds makes the net TOA fluxes more negative because of increased SW reflection (due to the larger optical depth) and increased LW emission (due to the lower height).

4. Computation of cloud feedback using cloud radiative kernels

Multiplying the cloud radiative kernel (K) by the change in cloud fraction histogram (ΔC) expressed in percent gives an estimate of the contribution of each cloud type to the change in TOA radiation associated with climate change (in this case, a doubling of CO_2):

$$\Delta R = K\Delta C. \quad (2)$$

For a given grid point and month, ΔC is multiplied by the cloud radiative kernel that corresponds to the control climate's clear-sky surface albedo for that location and month. Because the kernel is computed using the atmospheric and surface conditions from the control climate, the change in TOA fluxes computed in this manner is due solely to the change in clouds (i.e., no clear sky flux changes are included), which is the quantity relevant for cloud feedback. Dividing this response by the change in global mean surface air temperature ($\Delta \overline{T}_s$) provides an estimate of the cloud feedback (f) due to changes in the amount of each cloud type:

$$f = \frac{\Delta R}{\Delta \overline{T}_s}. \quad (3)$$

Note that f and ΔR are both functions of CTP, τ , latitude, longitude, and month. Summing f over all cloud types produces an estimate of the local contribution to the cloud feedback, which can then be averaged over the entire planet and over all months to compute the global and annual mean cloud feedback.¹ Unless otherwise

¹ Hereafter we refer to the radiative perturbations brought about by cloud changes as cloud feedback, with the implicit assumption that the simulated changes in clouds evolve with the change in global mean surface temperature. Gregory and Webb (2008) have provided evidence that a portion of the cloud-induced radiation response that is typically considered cloud feedback actually occurs due to very rapid tropospheric adjustment following a step change in CO_2 concentration, and that the portion due to cloud changes that evolve with temperature (i.e., the true cloud feedback) may be smaller in magnitude and even opposite in sign. CFMIP1 data do not permit us to distinguish between these two types of cloud changes; thus, what we refer to as cloud feedback may be a combination of these effects.

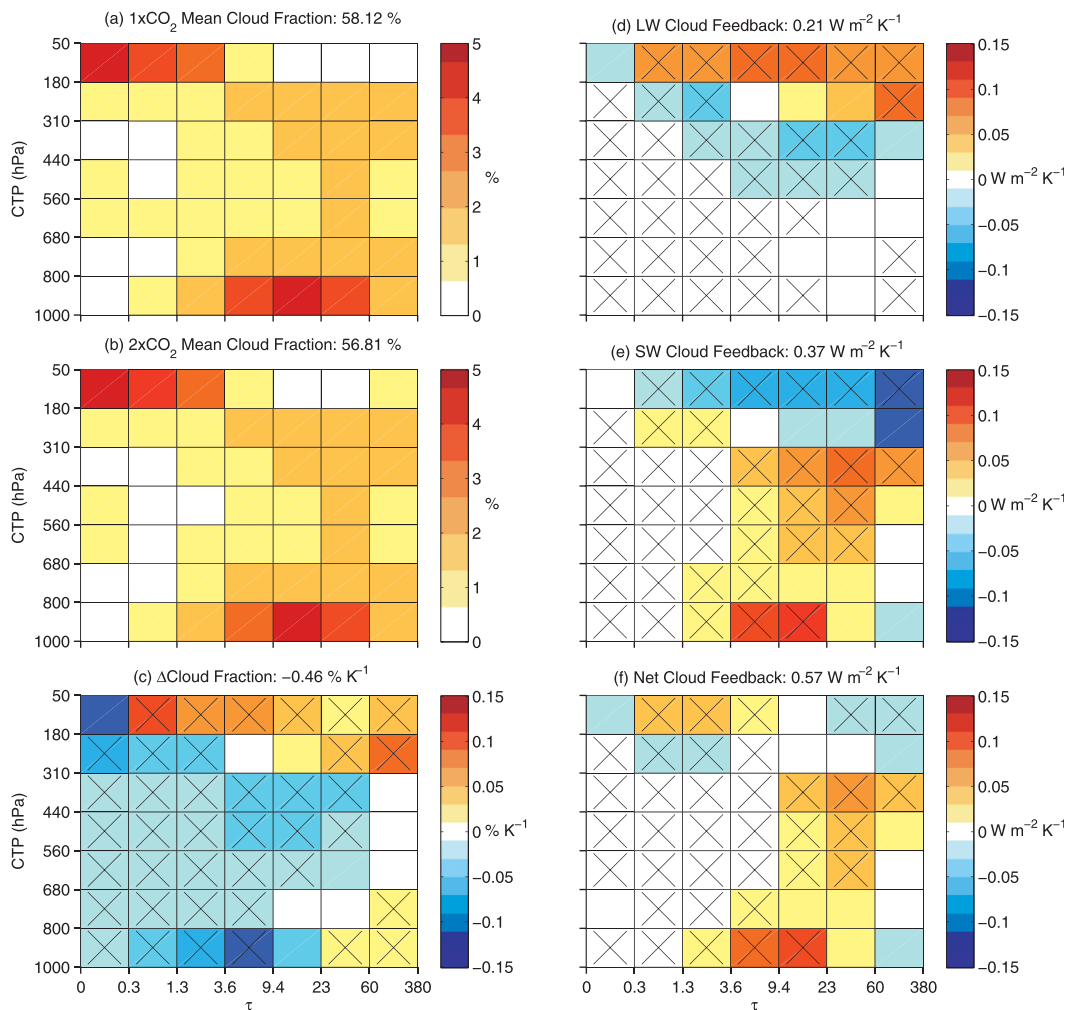


FIG. 2. Global, annual, and ensemble mean cloud fraction for the (a) $1 \times \text{CO}_2$ and (b) $2 \times \text{CO}_2$ runs, along with (c) the average difference expressed per unit change in each model's global mean surface air temperature between the two states. Matrix resulting from multiplying the change in cloud fraction at each location and month with the collocated (d) LW, (e) SW, and (f) net cloud radiative kernels, then taking the global, annual, and ensemble mean. The sum of each matrix is shown in each title. Bins containing an "x" indicate those in which $\geq 75\%$ of the models agree on the sign of the field plotted.

noted, all results hereafter are for annual mean quantities.

In the left column of Fig. 2 we show histograms of (Fig. 2a) $1 \times \text{CO}_2$ and (Fig. 2b) $2 \times \text{CO}_2$ global mean cloud fraction for the average of all models except MPI ECHAM5, along with (Fig. 2c) the difference in the cloud fraction expressed per unit change in each model's global mean surface air temperature between the two states. Bins containing an "x" indicate those in which $\geq 75\%$ of the models (i.e., 9 out of 11) agree on the sign of the field plotted. The MPI ECHAM5 model is excluded for reasons discussed in appendix A. Global mean cloud fraction decreases by $0.46\% \text{ K}^{-1}$ in the ensemble average, with individual models having decreases

ranging from 0.02 to $0.91\% \text{ K}^{-1}$. Robust reductions in cloud fraction occur in a majority of CTP and τ bins. Large reductions in cloud fraction occur in the highest CTP bin (i.e., the lowest clouds) in the $0.3 < \tau \leq 9.4$ range. Cloud fraction robustly increases in the lowest CTP bin (i.e., the highest clouds) at all optical depths except for τ between 0 and 0.3. Cloud fraction also increases in the 680–1000 hPa CTP bins for τ greater than 23 and in the 180–310 hPa CTP bin for τ greater than 3.6. That nearly every bin of (Fig. 2c) contains an "x" indicates that this distribution of global mean cloud fraction anomalies is quite robust across models.

Multiplying ΔC with the LW, SW, and net K matrices shown in Fig. 1 produces the contribution of each cloud

type to the respective feedbacks (Figs. 2d,e,f). Note that the multiplication occurs for each location, month, and model and is then averaged for this figure. Because the ISCCP simulator produces cloud fields only during sunlit months, a potential bias exists in the LW cloud feedback computed by this multiplication, but we find that it is small (appendix B).

The large increases in cloud fraction in the upper-troposphere project strongly onto the LW cloud radiative kernel, which is most sensitive to cloud fraction changes in the lowest CTP bins. The contribution to the LW cloud feedback is positive for bins in which cloud fraction increases and negative for bins in which cloud fraction decreases. Cloud fraction increases, primarily those occurring in the lowest CTP bin (i.e., the highest clouds), contribute $0.56 \text{ W m}^{-2} \text{ K}^{-1}$ to the LW cloud feedback, while cloud fraction decreases oppose this by $0.36 \text{ W m}^{-2} \text{ K}^{-1}$, resulting in a global and ensemble mean LW cloud feedback due to all cloud fraction changes of $0.21 \text{ W m}^{-2} \text{ K}^{-1}$. Across models, the global mean LW cloud feedback ranges from -0.13 to $0.69 \text{ W m}^{-2} \text{ K}^{-1}$.

In contrast to the LW cloud feedback, cloud changes throughout the depth of the troposphere contribute to the SW cloud feedback, which is $0.37 \text{ W m}^{-2} \text{ K}^{-1}$ in the global and ensemble mean. Large positive contributions come from bins in which cloud fractions decrease, and large negative contributions come from bins in which cloud fractions increase. Cloud fraction changes project more strongly onto the SW cloud radiative kernel if they occur at higher optical depths; thus the effect of cloud fraction changes in the lowest τ bins—though systematically positive across models—are small and less relevant for the SW cloud feedback. Across models, the global mean SW cloud feedback ranges from -0.18 to $0.93 \text{ W m}^{-2} \text{ K}^{-1}$.

The net cloud feedback matrix shares features of both the LW and SW matrices but is largely dominated by the positive SW cloud feedback for all pressures greater than about 310 hPa due to reductions in low and midlevel cloud fraction where the LW kernel is small. At pressures less than 310 hPa, LW and SW cloud feedback components compete against each other. The increase in cloud fraction in the lowest CTP bin contributes more strongly to the positive LW cloud feedback than to the negative SW cloud feedback for intermediate optical depths, but the opposite is true for thick high clouds. In the end, large reductions in middle- and low-level clouds, which strongly reduce the amount of reflected radiation, coupled with increases in high level clouds, which strongly reduce the amount of emitted LW radiation result in a net cloud feedback of $0.57 \text{ W m}^{-2} \text{ K}^{-1}$. Across models, the global mean net cloud feedback ranges from 0.16 to $0.94 \text{ W m}^{-2} \text{ K}^{-1}$. For comparison,

the global and ensemble mean combined water vapor plus lapse rate feedback we compute using the radiative kernels of Soden et al. (2008) ranges from 1.18 to $1.42 \text{ W m}^{-2} \text{ K}^{-1}$.

5. Effectiveness of the cloud radiative kernel method in computing cloud feedback

In this section we compare the cloud feedback computed using the cloud radiative kernels applied to ISCCP simulator output with the cloud feedback computed according to Shell et al. (2008) and Soden et al. (2008). The latter technique involves adjusting the change in cloud radiative forcing by the amount of cloud masking that occurs in the other feedbacks and in the radiative forcing. Only the HadSM4, HadSM3, HadGSM1, UIUC, MIROC(lowres), and AGCM4.0 models archived enough data to compute the adjusted change in cloud radiative forcing; thus, we can only compare the two methods for those models.

In Fig. 3 we show a point-by-point comparison of the LW and SW cloud feedbacks computed using cloud radiative kernels with those computed by the adjusted change in cloud radiative forcing method. Each point represents the feedback computed for a single month at a single location in the model, and locations in which the magnitude of the change in clear-sky surface albedo exceeds the 90th percentile have been removed (for reasons discussed below). Values of both LW and SW cloud feedback computed using the cloud radiative kernels developed here compare remarkably well on a point-by-point basis with values computed by adjusting the change in cloud radiative forcing. The regression slopes lie within 5% of the one-to-one line for the SW (except for the UIUC model) and within 15% in the LW [except for the MIROC(lowres) model]. Here, R^2 values greater than 75% for all but the MIROC(lowres) model indicate that these two measures are highly correlated, though LW correlations are systematically lower than SW correlations in every model. In all but the AGCM4.0 model, the cloud radiative kernel-derived magnitude of the local LW cloud feedback value is less than the local adjusted change in LW cloud radiative forcing magnitude (i.e., the kernel value is less positive where the feedback is positive and less negative where the feedback is negative; thus, the slopes in Figs. 3a–e are all <1).

Three prominent discrepancies between the two estimates of cloud feedback appear in this figure. First, the slopes between the two estimates of cloud feedbacks in the UIUC model deviate substantially from unity (Figs. 3d,j), especially in the SW. The cause of this discrepancy may reflect differences between the radiative transfer model used in the UIUC model and the

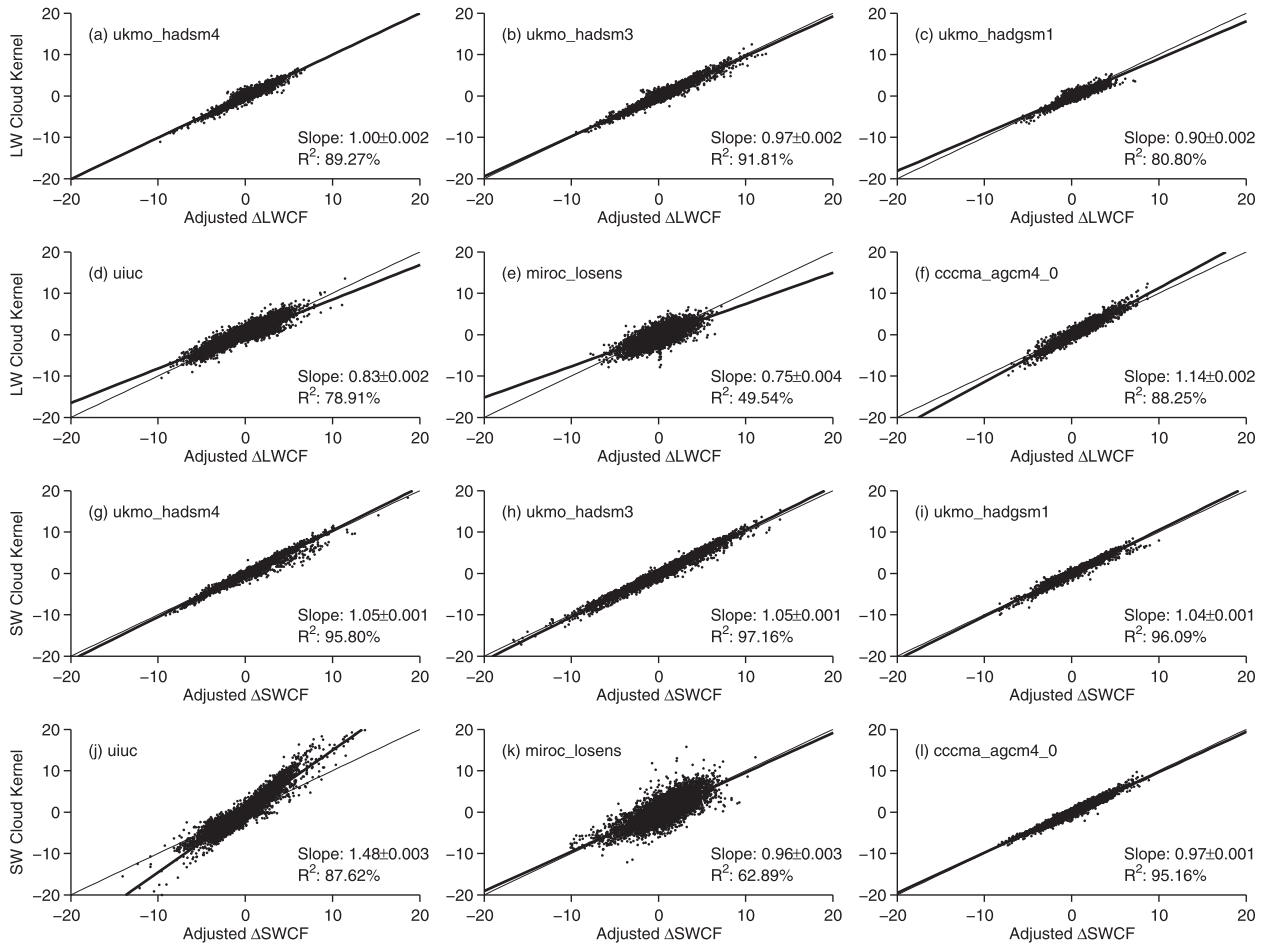


FIG. 3. Point-by-point comparison of (a)–(f) LW and (g)–(l) SW cloud feedbacks estimated from adjusting the change in cloud radiative forcing using kernels computed in Soden et al. (2008) (x axis) plotted against those estimated using the cloud radiative kernels developed here (y axis). Locations in which the magnitude of the change in clear-sky surface albedo exceeds the 90th percentile have been removed. The thin line is the one-to-one line, and the thick line is the linear least squares fit to the data. The slope and 2σ range of uncertainty of this regression line along with the fraction of variance explained by the fit are provided in each panel. The uncertainty is calculated from a bootstrapping method in which the residuals from the regression slope are resampled with replacement 1000 times to compute a distribution of possible regression coefficients.

Fu-Liou model used in generating the kernels. Second, the slope between the two estimates of LW cloud feedback in the MIROC(lowres) model is much less than 1, and the two estimates of LW and SW cloud feedbacks are less well-correlated than for the other models (Figs. 3e,k). This may arise in part because relevant diagnostics are archived for nonoverlapping time periods in the MIROC(lowres) model, so the adjusted change in cloud forcing is computed using differences between two climate states that are different from the two climate states used to perform the cloud radiative kernel computation. Furthermore, whereas 20-yr mean cloud fraction histograms are differenced in the other models to compute cloud feedbacks, the ISCCP simulator output is archived for only a brief 5-yr period for both runs of this model, likely worsening the signal-to-noise

ratio in its cloud radiative kernel-derived cloud feedbacks relative to those of other models. Third, the slope between the two LW cloud feedback estimates in the AGCM4.0 model (Fig. 3f) is much greater than 1. In this model, cloud optical depths passed to the radiation code are scaled relative to those passed to the ISCCP simulator; thus, we scaled both the LW and SW kernels in a manner consistent with how this model's clouds are scaled for SW radiative calculations (see appendix A). The somewhat larger slope in Fig. 3f likely reflects our choice to scale the LW kernel in the same manner as the SW kernel even though a different scaling of cloud optical depths (one that cannot be generally applied) was used for LW fluxes in this model.

Our comparisons between the two methods indicate poor agreement in some models over regions in which

clear-sky surface albedo changes significantly between the two climate states (e.g., over the Himalayas). Visual inspection of feedback maps (not shown) indicates that a large percentage of these points come from regions with high surface albedo in the $1 \times \text{CO}_2$ climate, where the adjusted change in cloud forcing method produces anomalous SW cloud feedbacks surrounded by regions with oppositely signed SW cloud feedbacks. The cloud radiative kernel–derived feedback values, on the other hand, exhibit a relatively “smooth” geographic distribution in these regions that is arguably more realistic. Whereas the cloud radiative kernel method computes cloud feedback directly from the change in cloud fraction with no influence from noncloud fields, the method of Shell et al. (2008) and Soden et al. (2008) requires adjusting the change in cloud forcing by the cloud masking of noncloud feedbacks, which may be problematic where surface albedo changes are large and the amount of cloud masking may vary considerably among models. Thus, we argue that the cloud radiative kernels developed here are more accurate in regions where surface albedo changes significantly, and we exclude from Fig. 3 locations in which the magnitude of the change in clear-sky surface albedo exceeds the 90th percentile.

In Fig. 4 we show the cloud radiative kernel–derived computation of global mean LW, SW, and net cloud feedbacks scattered against the estimates derived using the adjusted change in cloud radiative forcing method. We compare against estimates of adjusted change in cloud forcing derived using both the GFDL-based (Soden et al. (2008)) and CAM-based (Shell et al. 2008) radiative kernels to indicate some measure of the uncertainty in that method. In the global mean, cloud radiative kernel–derived estimates of both LW and SW cloud feedbacks are smaller than the adjusted change in LW and SW cloud radiative forcing (ΔLWCF and ΔSWCF , respectively) in five out of six models. For LW cloud feedback estimates, closer agreement is found with the Shell et al. (2008) kernels than with the Soden et al. (2008) kernels, but the opposite is true in the SW. Excluding the UIUC model, it is clear that global mean LW and SW cloud feedbacks calculated using the two techniques are well correlated, but the net cloud feedbacks computed with the cloud radiative kernels tend to be less than the adjusted ΔNetCF cloud feedback, and this is primarily caused by discrepancies in the LW term.

Cloud feedback estimates for the UIUC model stand out as particularly anomalous in this comparison. It is noteworthy, however, that this model only appears anomalous when its cloud radiative kernel–computed feedbacks are compared with the adjusted change in cloud radiative forcing, not when they are compared

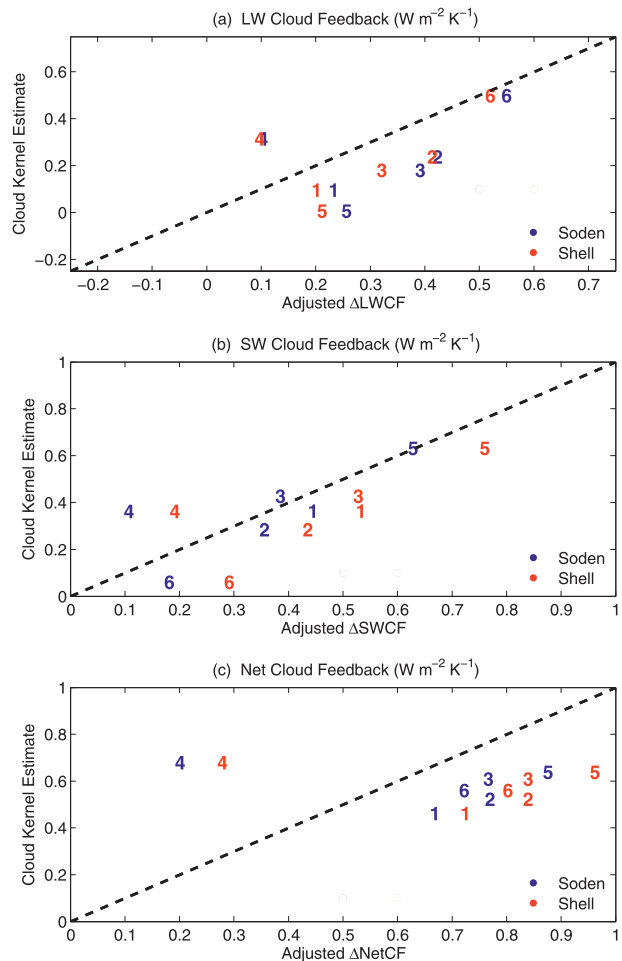


FIG. 4. Global and annual mean (a) LW, (b) SW, and (c) net cloud feedbacks for the (1) HadSM4, (2) HadSM3, (3) HadGSM1, (4) UIUC, (5) MIROC(lowres), and (6) AGCM4.0 models estimated using the cloud radiative kernels developed here (y axis) plotted against estimates from adjusting the change in cloud radiative forcing using the radiative kernels developed by (blue) Soden et al. (2008) and (red) Shell et al. (2008) (x axis). The dashed line is the one-to-one line. Note that the x axis and y axis limits vary from panel to panel, but all span a range of $1 \text{ W m}^{-2} \text{ K}^{-1}$.

with the cloud radiative kernel–computed feedbacks of the other models. Cloud feedbacks computed using the cloud radiative kernels (which rely on a standard radiative transfer code and a standard definition of cloud) are in better agreement across models than feedbacks computed from adjusting the change in cloud forcing (which relies in part on the cloud radiative forcing computed in each model’s radiative transfer scheme). This suggests that the discrepancy arises because of anomalous features in the way that the UIUC model’s radiative transfer scheme calculates the radiative impact of a cloud with a given value of CTP and τ relative to that of other models and to that of the Fu–Liou scheme used in generating our kernel. Indeed, Tsushima et al. (2006)

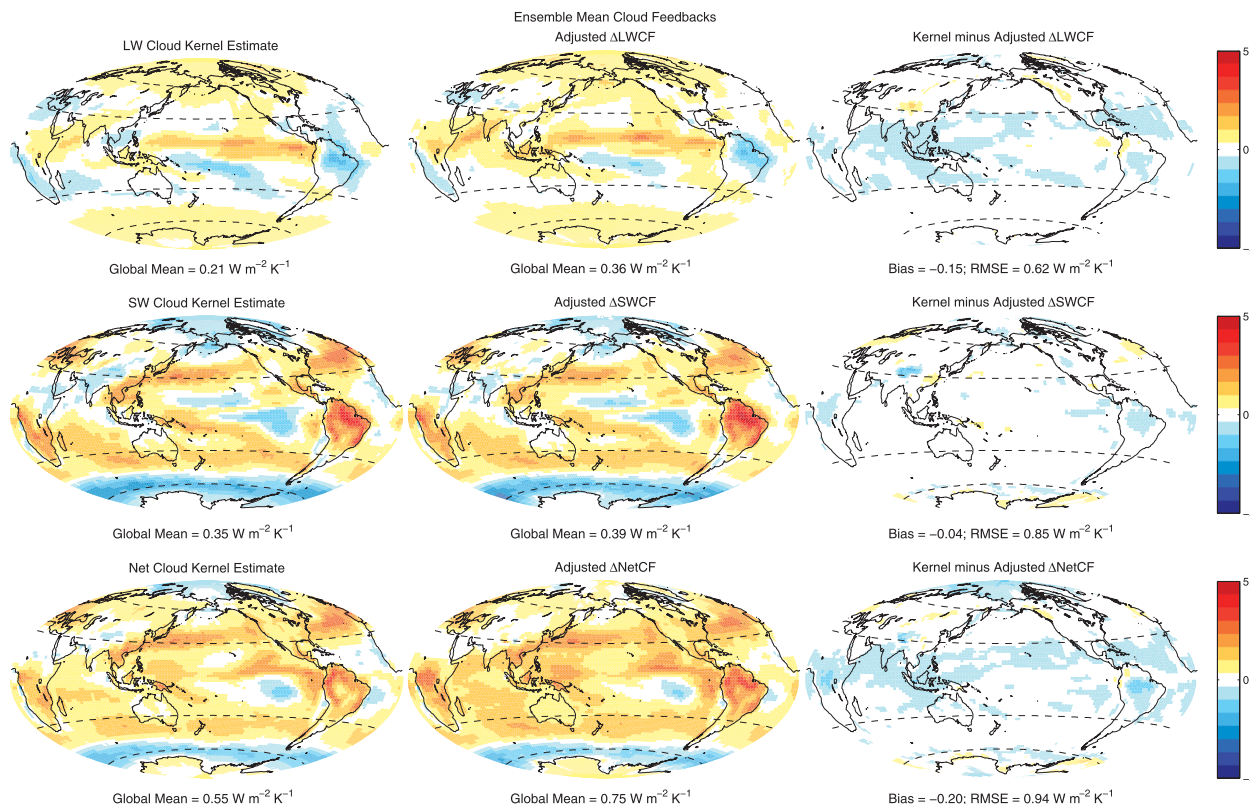


FIG. 5. Estimates of annual and ensemble mean (top) LW, (middle) SW, and (bottom) net cloud feedback derived using (left) cloud radiative kernels and (middle) the adjusted change in cloud forcing derived with kernels computed in Soden et al. (2008), along with (right) the difference between the two estimates. The ensemble refers to models in which the standard kernel calculation is possible but excluding the UIUC model. The root-mean-squared error is computed by differencing the maps of the two feedback estimates for each month in each model, squaring the values, averaging in space and across months and models, then taking the square root.

noted that this model has the lowest cloud albedo forcing despite having the largest total water content among the five models they analyzed. Considering that the adjusted change in cloud forcing estimate is constrained by the actual TOA flux anomalies produced by the model, it is likely that it gives the more accurate value of cloud feedback within a particular model (though we find that the clear-sky LW and SW TOA flux anomalies produced by these models differ from those estimated by summing the Shell et al. (2008) and Soden et al. (2008) kernel-derived fluxes by amounts of roughly 15% and 7%, respectively). However, the results shown in Fig. 4 for the UIUC model highlight an important advantage of the cloud radiative kernel method: The intermodel spread in this technique can unambiguously be attributed to differences in cloud responses (aside from the small spread arising from different mean-state surface albedos discussed in appendix B). In contrast, the spread in adjusted change in cloud forcing estimates includes intermodel differences in radiation schemes. (Note that this is not true for the noncloud feedbacks computed using that technique.)

In Fig. 5 we show the spatial structure of the ensemble mean cloud feedbacks computed with the cloud radiative kernels (left column) and computed by adjusting the change in cloud forcing (middle column) with the Soden et al. (2008) kernels averaged across the HadSM4, HadSM3, HadGSM1, MIROC(lowres), and AGCM4.0 models. The difference maps are also provided in the right column. The UIUC model is excluded from the ensemble means plotted in this figure because of the anomalous behavior identified above.

The net cloud feedback is generally positive between 50°S and 60°N, exceptions being just south of the equator in the eastern Pacific, in the subtropical Atlantic, and over the Tibetan Plateau. The low-latitude signal is dominated by the SW cloud feedback, but the positive LW cloud feedback on the equator in the Pacific contributes significantly to the positive net cloud feedback there. Large positive SW cloud feedback outweighs large negative LW cloud feedback over the Amazon, in the South Pacific Convergence Zone and over southern Africa. Negative SW cloud feedback outweighs positive LW cloud feedback in the Southern Ocean region.

It is clear that both techniques produce global feedback patterns that are very similar and it is difficult to visually discern differences in the patterns between the left and middle columns. Global and ensemble mean SW cloud feedback estimates are in better agreement between the two techniques than those in the LW, but RMS differences are larger in the SW. Cloud radiative kernel–derived estimates of both LW and SW cloud feedbacks are less than the adjusted change in cloud forcing estimates in the global and ensemble mean, leading to a net difference of $-0.20 \text{ W m}^{-2} \text{ K}^{-1}$. When the CAM-based kernels (Shell et al. 2008) are used in place of the GFDL-based kernels (Soden et al. (2008)), the LW difference is reduced, the SW and net differences are increased, and all RMSE values increase. Inclusion of the UIUC model in the ensemble mean reduces the global mean differences but increases the root mean squared difference between the two estimates of LW, SW, and net cloud feedback.

In light of all the results presented in this section, we argue that as long as a model does not have a radiation code that calculates cloud radiative effects drastically different from the Fu–Liou code used to generate the kernels, and as long as the ISCCP simulator is implemented properly, the cloud radiative kernel technique works remarkably well in computing cloud feedback. To the extent that a given model’s radiation code varies from Fu–Liou, the cloud feedback computed with this technique will not be the exact cloud feedback “felt” in that model, and if one seeks highly accurate diagnosis of that true cloud feedback, other methods may be more appropriate. If one seeks to perform an intercomparison of cloud feedbacks where the spread is unambiguously attributable to differences in the response of clouds, the method proposed here is superior. Finally, if one seeks to quantify across different models the contributions of different cloud types to cloud feedback (as we demonstrate in the following section), this technique is the only choice.

6. Partitioning cloud feedback by cloud types

Cloud radiative kernels allow one to directly attribute the contributions of specific cloud types to the cloud feedback at each location. Rather than documenting the feedbacks due to each of the 49 cloud types, hereafter we will consider the feedbacks due to cloud changes within the commonly-used ISCCP cloud-type classifications of Rossow and Schiffer (1999)—namely low: $680 < \text{CTP} \leq 1000 \text{ hPa}$; middle: $440 < \text{CTP} \leq 680 \text{ hPa}$; high: $50 < \text{CTP} \leq 440 \text{ hPa}$; thin: $\tau \leq 3.6$; medium: $3.6 < \tau \leq 23$; and thick: $\tau > 23$. Although some information is lost, it makes figures less unwieldy, and it better characterizes

the overall effect of changes in the major cloud types by summing over compensating changes within regions of the histogram (e.g., small changes in clouds moving among the bins, but remaining within certain major cloud types). Thus, feedbacks partitioned in this manner provide information about which representative cloud types contribute to the feedback, but not about the nature of the cloud changes occurring within that cloud type. Partitioning of cloud feedbacks into contributions from changing cloud-top altitude, optical depth, and total amount is performed in the companion paper to this study.

In Fig. 6 we show the zonal mean contribution of high, middle, and low clouds to the LW, SW, and net cloud feedbacks averaged across the ensemble of models. Henceforth, the ensemble refers to all models except the MPI ECHAM5 model, which is excluded for reasons discussed in appendix A. As expected based on the fact that the LW cloud radiative kernel magnitude increases with decreasing CTP, the LW cloud feedback is dominated at all latitudes by the response of high clouds (Fig. 6a). However, fewer than 75% of the models agree on the sign of the high cloud contribution to the LW cloud feedback at most tropical latitudes, as indicated by the dashed lines in these regions. As will be shown in Part II, this is primarily because of two robust but opposing effects: increases in high cloud altitude (a positive effect) and decreases in high cloud fraction (a negative effect). In the extratropics, the high cloud contribution is systematically positive across models. Low cloud changes are irrelevant at all latitudes, but middle-level cloud changes robustly act to slightly reduce the LW cloud feedback in the mid-latitudes.

In contrast, cloud changes at all altitudes are relevant for SW cloud feedback at all latitudes (Fig. 6b). With the exception of the high latitudes, changes in low and middle level clouds contribute to a positive SW cloud feedback. High cloud changes contribute negatively to the SW cloud feedback in the global mean, but most prominently in the deep tropics (due mainly to large increases in high cloud fraction over the Equatorial Pacific) and poleward of about 40° in both hemispheres, the latter feature being more robust. The effect of changes in high clouds in the deep tropics strongly opposes the effect of changes in the other cloud types, producing a local minimum in the zonal mean SW cloud feedback. Positive SW cloud feedbacks from the middle level cloud response are roughly 80% as large as those from the low level cloud response in the global mean and are larger in the middle and high latitudes, a result that is not generally acknowledged and is frequently overshadowed by the

focus on feedback spread arising from subtropical low cloud changes.²

Cloud changes in every height category contribute positively to the net cloud feedback (Fig. 6c), and the zonal mean net cloud feedback is robustly positive between about 50°S and 60°N. Because of their largely compensatory effects on the SW and LW cloud feedbacks, high cloud changes contribute less than low cloud changes to the net cloud feedback at all latitudes. Mid-level cloud changes, which primarily contribute to the SW cloud feedback, contribute roughly the same amount to the global net cloud feedback as high cloud changes and have a very similar latitudinal distribution, except in high southern latitudes. Middle- and high-level cloud changes together are responsible for more than half of the global and ensemble mean net cloud feedback.

In Fig. 7 we show the ensemble mean zonal mean contribution of thin, medium, and thick cloud changes to the LW, SW, and net cloud feedbacks. In the global mean sense, thick cloud changes dominate the LW cloud feedback, particularly at high latitudes (Fig. 7a). In the ensemble mean, cloud changes in all three thickness categories contribute equally to the large positive LW cloud feedback in the deep tropics (7.5°S–15°N), but the sign of this feature is not robust across models. Poleward of about 50° in either hemisphere, the robustly positive contribution from thick cloud changes is only slightly opposed by thin cloud changes, making the LW cloud feedback large and robustly positive.

In the global mean, the positive SW cloud feedback arises primarily because of medium thickness cloud changes, which contribute positively everywhere but over the poles (though the sign of this contribution is not robust between about 20°S and 10°N; Fig. 7b). Although they make a robustly positive contribution at high latitudes, thin cloud changes contribute minimally to the

SW cloud feedback. Thick cloud changes are at least as important at most latitudes as medium thickness cloud changes and with greater robustness. However, whereas medium thickness cloud changes contribute positively almost everywhere, the thick cloud contribution is positive equatorward of about 45° and strongly negative elsewhere, such that thick cloud changes make almost no contribution to the global mean SW cloud feedback. The sharp decrease in the SW cloud feedback with latitude in the midlatitudes is entirely caused by changes in thick clouds and is generally opposed by smaller cloud fraction changes in the other τ categories. Particularly striking is the negative feedback in the Southern Ocean region, which reaches a peak value of $-1.5 \text{ W m}^{-2} \text{ K}^{-1}$, with thick cloud changes alone contributing $-2.1 \text{ W m}^{-2} \text{ K}^{-1}$. This feature will be discussed in greater detail in Part II.

Cloud fraction changes in all optical depth categories contribute positively to the global mean net cloud feedback, with the medium thickness cloud changes dominating due to their uniformly positive contributions (Fig. 7c). Equatorward of about 40°, thick and medium thickness cloud changes contribute about equally to the net cloud feedback, with thick cloud changes primarily causing the abrupt latitudinal transition from positive to negative cloud feedback in the midlatitudes.

In Fig. 8 we show ensemble mean global mean cloud feedback estimates and their partitioning among high, middle, low, thin, medium, and thick cloud changes. Note that the total cloud feedback given in the left-most column is equal to both the sum of the high, middle, and low cloud feedbacks and the sum of the thin, medium, and thick cloud feedbacks. Cloud feedbacks partitioned by altitude ranges should not be summed with those partitioned by optical depth ranges because double-counting would occur. In this ensemble of 11 models, 65% of the net cloud feedback comes from the SW cloud feedback and 35% from the LW. For both the global mean SW and LW cloud feedbacks, only one model has negative values (not the same model). Considerable spread is evident in both the LW and SW components of cloud feedback, though the spread is larger in the SW. Anticorrelation between LW and SW cloud feedback estimates across models results in the net cloud feedback having less intermodel spread than that of SW cloud feedback, and no models exhibit a negative net cloud feedback.

As mentioned previously, LW cloud feedback is dominated by the response of high clouds, with middle and low clouds making small negative contributions. Cloud changes at all vertical levels contribute to the SW cloud feedback, with high cloud changes generally contributing negatively and middle and low cloud changes contributing

² A well-known tendency of the ISCCP retrieval algorithm that is purposely built into the simulator is to identify a single cloud with a CTP at midlevels for scenes in which thin high clouds overlap low clouds (e.g., Jin and Rossow 1997; Stubenrauch et al. 1999). Motivated by a concern that the significant midlevel cloud feedback we have inferred may arise partly due to clouds that are not actually at midlevels, we compared high, middle, and low cloud amounts derived from the histogram and from the model-level cloud fraction diagnostic provided by seven modeling centers. We found that the sign of midlevel cloud changes defined by both diagnostics is consistent for 86% of all points, which is comparable to the 87% for high clouds and 83% for low clouds. Furthermore, for the small number of grid points in which the signs differ, the number of positive histogram-derived midlevel cloud fraction anomalies is roughly equal to the number that are negative, implying no systematic disagreement. Although this is a crude comparison, it shows that, over the vast majority of grid points, middle-level cloud changes are indeed causing midlevel cloud feedbacks.

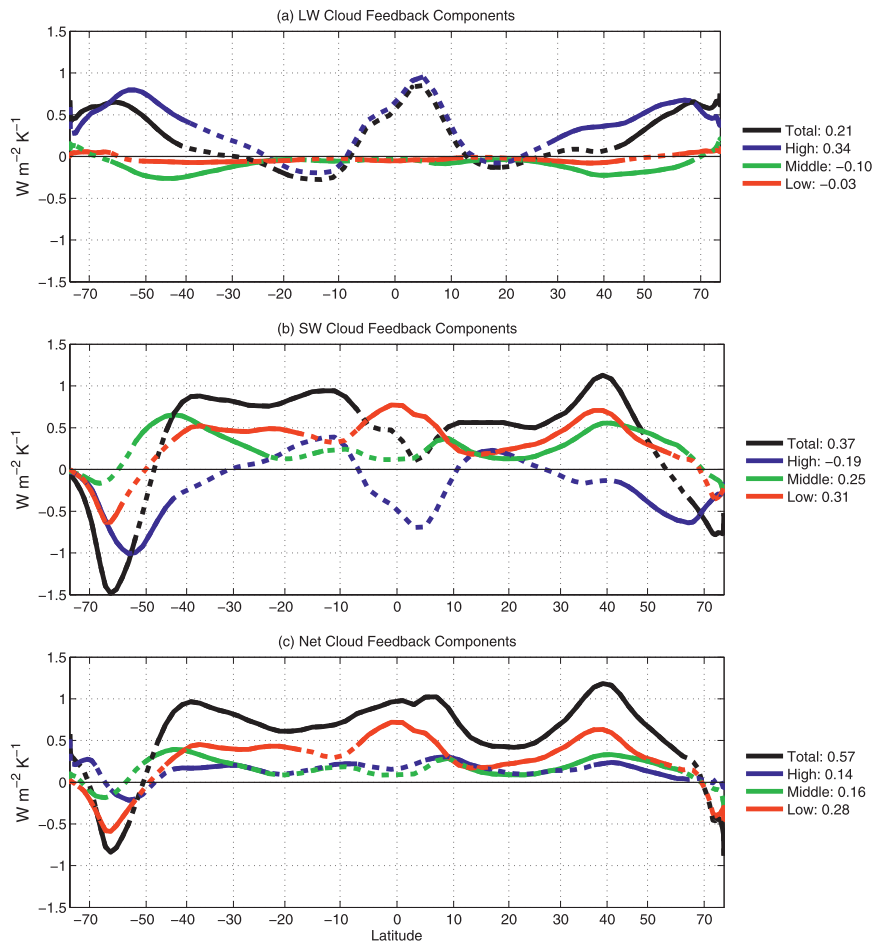


FIG. 6. Zonal, annual, and ensemble mean (a) LW, (b) SW, and (c) net cloud feedbacks partitioned into contributions from high, middle, and low cloud changes. Global mean values of each contribution are shown in the legend. Lines are solid where $\geq 75\%$ of the models agree on the sign of the field plotted, dashed elsewhere.

positively, in agreement with the results of Yokohata et al. (2010) from two perturbed physics ensembles of the MIROC3.2 and HadSM3 models. Considerable intermodel spread is evident in the contributions of clouds at all heights to the SW cloud feedback. Contributions of high, middle, and low cloud changes to the net cloud feedback exhibit appreciable spread, but are systematically positive. The spread is largest for low clouds, a result consistent with many previous studies (e.g., Bony and Dufresne 2005).

An important and generally unappreciated result shown in Fig. 8 is that the high cloud contribution to the intermodel spread in net cloud feedback is smaller than the contribution from low clouds not because the response of high clouds is small and/or consistent across models. Rather, the intermodel spread in the response of high clouds contributes substantial spread to both LW and SW cloud feedbacks. Specifically, the

contributions of high cloud changes to LW and SW cloud feedbacks each span a range of about $1 W m^{-2} K^{-1}$, whereas the contribution of low cloud changes to SW cloud feedback spans a range of only $0.6 W m^{-2} K^{-1}$. Because the spread in high cloud-induced LW and SW components is partially compensatory, however, the spread in net cloud feedback induced by high cloud changes is smaller than that induced by low cloud changes, for which no such compensation occurs.

Thin cloud changes generally make a small contribution to the feedback in all models. Thick cloud changes make a larger contribution to the positive LW cloud feedback than do medium thickness cloud changes, but the multimodel mean SW cloud feedback is dominated by medium thickness cloud reductions. Interestingly, all models exhibit a positive contribution to SW cloud feedback from medium-thickness cloud changes, whereas

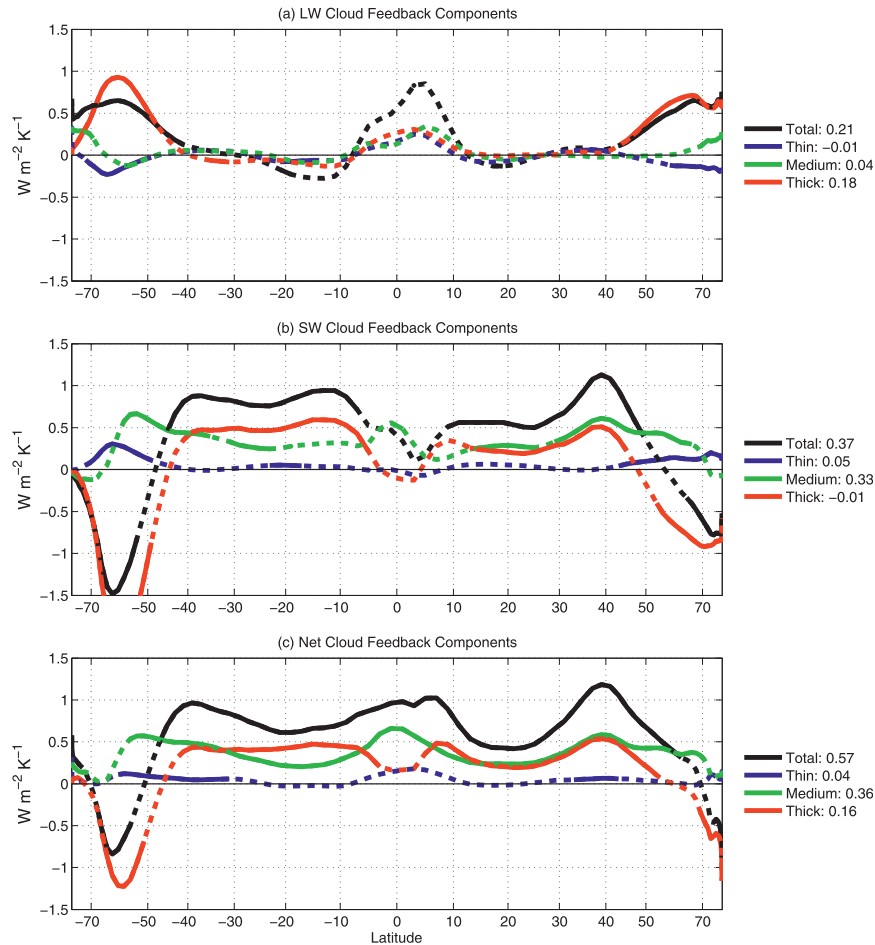


FIG. 7. As in Fig. 6, but partitioned into contributions from thin, medium, and thick cloud changes.

roughly an equal number of models exhibit positive and negative SW cloud feedback contributions from thick cloud changes. Conversely, all models exhibit positive contribution to LW cloud feedback from thick cloud changes, whereas roughly an equal number of models exhibit positive and negative LW cloud feedback contributions from medium-thickness cloud changes. These features can be explained simply by the spatial structure of these feedback components: feedbacks whose global mean value is the smaller residual of large and opposing values (i.e., LW medium, SW thick) are sensitive to the relative sizes of the areas of negative and positive feedback whereas those in which the feedback has a consistent sign in space (i.e., LW thick, SW medium) will have a robust sign across models. A clear example is the SW cloud feedback due to thick cloud changes, for which the lower latitude contribution is nearly exactly compensated by the higher-latitude contribution (Fig. 7b). Models in which the latitude of the transition from positive to negative contributions occur farther

equatorward (poleward) than in the ensemble mean have negative (positive) global mean SW thick cloud feedbacks.

The spread in SW cloud feedback due to both medium and thick cloud types is large, but because the SW cloud feedback is systematically positive for medium thickness clouds, it represents the largest positive contribution to the ensemble mean cloud feedback of all thickness categories. Indeed, medium-thickness cloud changes represent the single most important contributor to the ensemble mean positive net cloud feedback.

7. Conclusions

In this paper we demonstrated a new method of computing cloud feedbacks in models that output simulated cloud fractions as functions of cloud-top pressure and cloud optical depth. ISCCP simulator-produced cloud fields have a distinct advantage over the standard cloud fraction profile diagnostic in that they are

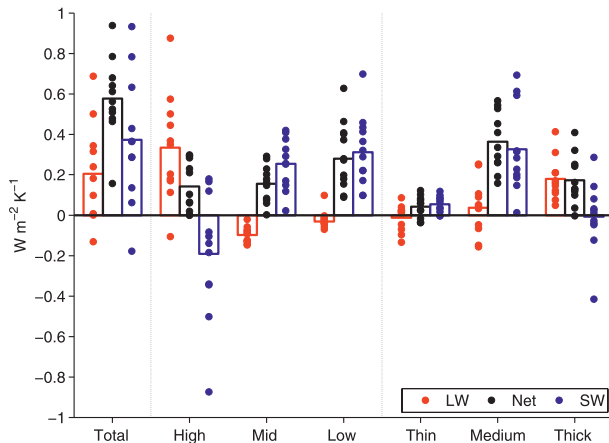


FIG. 8. Global and annual mean (red) LW, (black) net, and (blue) SW cloud feedback estimates and the contribution to the cloud feedbacks from changes in high, middle, low, thin, medium, and thick clouds. Each model is represented by a dot and the ensemble mean is represented by the height of the vertical bar.

defined consistently across models and represent the “radiatively-relevant” cloud tops that are directly impacting TOA fluxes. The latter property allows us to compute TOA flux sensitivities for cloud fraction fluctuations within each CTP and τ bin in the ISCCP histogram. To do so, we generate cloud radiative kernels by differencing overcast- and clear-sky TOA fluxes produced by the Fu-Liou radiative transfer model run with and without synthetic cloud condensate profiles appropriate for each CTP- τ bin.

Cloud feedback is computed using the kernels in a similar manner to the computation of standard feedbacks as in Shell et al. (2008) and Soden et al. (2008). Specifically, at every location in the model, the change in cloud fraction in each CTP- τ bin between the doubled- CO_2 run and control run is multiplied by the corresponding cloud radiative kernel for that bin. The feedback is computed by summing over all CTP and τ bins and dividing by the global mean surface air temperature change.

Several appealing aspects of this technique are worth highlighting. First, cloud feedbacks are computed directly from the change in cloud fields, which means the contributions to the feedback from specific cloud types are computed rather than inferred. Second, cloud feedbacks are computed using the same kernel across models, which isolates the role of cloud changes in driving intermodel differences in feedback values, without any model-to-model variation in how a radiative transfer code computes the radiative effects of a given cloud. Third, only monthly mean ISCCP simulator output is needed to compute the feedback, which makes it a very straightforward calculation, one that does not require extracting instantaneous cloud output to implement the

partial radiative perturbation technique (Wetherald and Manabe 1980) or adjusting the change in cloud forcing by the amount of masking in all other feedbacks. Finally, our technique cleanly removes clear-sky changes that are irrelevant for cloud feedback but may be difficult to remove using other techniques, resulting in TOA flux anomalies that are solely due to changes in the cloud fraction histogram.

We have demonstrated that cloud feedbacks computed with the cloud radiative kernels compare favorably with values computed by adjusting the change in cloud radiative forcing (Shell et al. 2008; Soden et al. 2008). On a point-by-point basis, cloud feedbacks computed using the two methods lie within 5% of the one-to-one line for the SW (except for the UIUC model) and within 15% in the LW [except for the MIROC(lowres) model]. Furthermore, R^2 values are greater than 75% in every model except the MIROC(lowres) model. Although the ensemble (five-model) mean cloud feedback spatial patterns are very similar, global mean cloud feedbacks estimated using cloud radiative kernels are slightly smaller in magnitude than those estimated by adjusting the change in cloud forcing, especially in the LW.

We find that changes in high clouds make the largest contribution of any cloud type to the LW cloud feedback at all latitudes in the 11-model ensemble mean, especially in the deep tropics. This is consistent with the structure of the LW cloud radiative kernel, which indicates that the sensitivity of OLR to cloud fraction changes increases with decreasing cloud-top pressure. However, because high cloud increases contribute negatively to the SW cloud feedback, their contribution to the net cloud feedback is considerably reduced. In contrast, low cloud changes, which only impact the SW cloud feedback, make a larger contribution to the net cloud feedback than cloud fraction changes at other altitudes. However, it is important to bear in mind that even for the global mean net cloud feedback, the positive contribution from the sum of middle- and high-level topped clouds slightly exceeds the contribution from low level clouds.

Cloud changes in all optical thickness categories contribute positively to the net cloud feedback, and increases in thick clouds at high latitudes in either hemisphere cause the large negative SW and net cloud feedbacks at latitudes poleward of about 50° . Although they exhibit considerable intermodel spread, contributions to SW and net cloud feedback from medium thickness clouds are systematically positive across models, making medium-thickness cloud changes the single most important contributor to the net cloud feedback.

In agreement with previous studies, we find that the spread in net cloud feedback is dominated by the contribution from low clouds. However, this result should

not be taken as evidence that high cloud changes have either a small or consistent impact on radiative fluxes across models. Rather, high cloud changes induce an even wider range of contributions to SW and LW cloud feedbacks than do low cloud changes, but partial compensation between the LW and SW impacts of high cloud changes reduces their contribution to the spread in net cloud feedback relative to that of low cloud changes.

In the companion to this paper, we propose a technique to decompose the change in cloud fraction within the ISCCP simulator histograms in such a way as to isolate the contributions to cloud feedback from changes in total cloud amount holding the vertical and optical depth distribution fixed, changes in altitude holding the optical depth distribution and total cloud amount fixed, and changes in optical depth holding the vertical distribution and total cloud amount fixed. This decomposition is performed to highlight the nature of cloud changes that give rise to cloud feedbacks and provides an indication of the physical processes that are important for both the mean and spread in cloud feedback across models.

Acknowledgments. We acknowledge the international modeling groups, the Program for Climate Model Diagnosis and Intercomparison (PCMDI), and the WCRP's Working Group on Coupled Modelling (WGCM) for their roles in making available the WCRP CFMIP multi-model dataset. Support of this dataset is provided by the Office of Science, U.S. Department of Energy. We thank Karen Shell and one anonymous reviewer for detailed critiques of this manuscript, Brian Soden and Karen Shell for providing radiative kernels, Rick Hemler for providing additional gfdl_mlm2_1 model output, Rob Wood, Chris Bretherton, and Robert Pincus for useful discussion and suggestions for improvement, and Marc Michelsen for computer support. This research was supported by the Regional and Global Climate Modeling Program of the Office of Science at the U. S. Department of Energy and by NASA Grant NNX09AH73G at the University of Washington. This work was performed under the auspices of the U.S. Department of Energy by Lawrence Livermore National Laboratory under Contract DE-AC52-07NA27344.

APPENDIX A

Verification of Proper ISCCP Simulator Implementation

a. Consistency between measures of total cloud fraction

To ensure proper implementation of the ISCCP simulator, modeling centers are expected to verify that the

total cloud fraction computed by summing the CTP- τ histogram is the same as the total cloud fraction diagnostic computed by the GCM cloud scheme. Here we perform this test using output from the CFMIP1 archive. In two models [BMRC1 and MIROC(hires)], the total cloud fraction diagnostic is not reported, so no comparison could be made. Since the cloud feedbacks computed for these two models also cannot be "ground-truthed" against the adjusted change in cloud forcing method, we cannot verify that the simulator is implemented properly in these models. However, in an effort to keep a reasonably-sized ensemble of models in our analysis, we take on faith that they have properly implemented the simulator. It is somewhat reassuring that their cloud fraction histograms are not anomalous relative to the ensemble mean.

RMS differences in the two measures of total cloud fraction are 8% in the IPSL CM4 model, 4% in the CCSM3.0 model, and less than 2% in the HadSM4, HadSM3, HadGSM1, UIUC, and AGCM4.0 models. Because these models had less than 10% RMS difference, we consider them to have satisfactorily implemented the simulator. We additionally wish to note that the 4% RMS difference in the CCSM3.0 model reflects the presence of "empty clouds" that are recorded by the model's cloud amount diagnostic but not by the simulator (B. Medeiros 2011, personal communication). Such "clouds" contain zero liquid water but are present due to the diagnostic cloud fraction being computed separately from the prognostic cloud water in CAM (Hannay et al. 2009). In these situations, the simulator is providing the true radiatively relevant clouds.

In the GFDL MLM2.1 model, the total cloud fraction computed by summing the CTP- τ histogram greatly underestimates (by about 25% absolute) the total cloud fraction diagnostic, and global mean RMS differences between the two fields are 24%. We found that the CTP- τ histogram for this model archived in the CFMIP1 database had not been divided by the fraction of radiation time steps with sunlit conditions. Dividing by the fraction of calls to the simulator in each month with sunlit conditions (data field provided by R. Hemler) brought the total cloud fractions into agreement, with an RMS difference of roughly 1%.

In the MIROC(lowres) model, the total cloud fraction computed by summing the CTP- τ histogram greatly overestimates (by about 25% absolute) the total cloud fraction diagnostic, and global mean RMS differences between the two fields are 29%. This is because this model's total cloud fraction diagnostic excludes clouds with τ less than 0.3 (Y. Tsushima, personal communication, 2011) that happen to have the greatest fractional coverage in this model. Summing the histogram

TABLE A1. Global mean LW and SW cloud feedbacks computed with the adjusted change in cloud forcing technique using the Shell et al. (2008) and Soden et al. (2008) kernels, and with the cloud radiative kernels developed in this study. The “Standard” column refers to values computed using the standard cloud radiative kernels (i.e., those in which the fluxes at all four corners of each CTP- τ bin are averaged before multiplication). “Min” and “Max” refer to the extreme values computed using four sets of kernels, each defined by fluxes computed at corners of each CTP- τ bin.

Model	Adjusted Δ LWCF		LW cloud radiative kernel			Adjusted Δ SWCF		SW cloud radiative kernel		
	Shell	Soden	Standard	Min	Max	Shell	Soden	Standard	Min	Max
HadSM4	0.19	0.22	0.10	0.01	0.19	0.52	0.44	0.37	0.27	0.46
HadSM3	0.40	0.41	0.24	0.17	0.29	0.43	0.35	0.29	0.23	0.35
HadGSM1	0.31	0.38	0.18	0.13	0.25	0.52	0.38	0.43	0.30	0.56
UIUC	0.09	0.09	0.32	0.28	0.34	0.18	0.10	0.36	0.26	0.47
MIROC(lowres)	0.20	0.25	0.01	-0.14	0.13	0.75	0.62	0.63	0.46	0.82
AGCM4.0	0.51	0.54	0.50	0.44	0.57	0.28	0.17	0.06	0.02	0.11
BMRC1	N/A	N/A	-0.13	-0.25	-0.03	N/A	N/A	0.29	0.17	0.40
GFDL MLM2.1	N/A	N/A	0.69	0.63	0.77	N/A	N/A	-0.18	-0.26	-0.09
IPSL CM4	N/A	N/A	0.00	-0.13	0.13	N/A	N/A	0.78	0.56	1.01
MIROC(hires)	N/A	N/A	0.00	-0.15	0.14	N/A	N/A	0.93	0.74	1.12
CCSM3.0	N/A	N/A	0.34	0.30	0.39	N/A	N/A	0.14	0.10	0.17

but excluding the clouds in the thinnest τ bin brought the two estimates of total cloud fraction into very close agreement, with an RMS difference of roughly 2%.

Finally, we have chosen to exclude the MPI ECHAM5 model from our analysis based on two considerations. First, the total cloud fraction as computed by summing its CTP- τ histogram is rarely less than 80% at any location on the planet, which is significantly different from the total cloud fraction diagnostic, with an RMS difference of 30.5%. The global mean total cloud fraction as computed from summing the histogram is a highly suspect 92%. Second, the RMS difference between this model’s CTP- τ histogram and the ensemble mean histogram is larger than for any other model in the ensemble, with values exceeding 10% in several bins. Williams and Webb (2009) have also noted that among the ten models they analyzed, the MPI ECHAM5 model’s histogram has the largest Euclidean distance to ISCCP observations in several cloud regimes.

b. Consistency between clouds and radiation

Unlike the typical implementation of the ISCCP simulator in which the cloud fields reported in the histogram represent those for which the radiative transfer calculations are performed, in the AGCM4.0 model, the cloud fields reported in the ISCCP simulator histogram are different from those used by the model’s radiation code (J. Cole, personal communication, 2011). In this model’s radiation calculations, cloud visible optical depths are scaled down according to Eq. (12) of Li et al. (2005) to account for subgrid-scale inhomogeneity in the cloud fields that strongly impacts scattering (Li 2000; Li and Barker 2002). Because the ISCCP simulator is called prior to this scaling, the cloud fields reported in the histogram do not represent the same clouds as

seen by that model’s radiation code. Thus, the GCM-produced radiative fluxes are guaranteed to be inconsistent with those computed using the cloud radiative kernels applied to ISCCP simulator output because the kernels assume the clouds in the histogram are those seen by the radiation. To partially circumvent this problem, for this model only we take the values of the cloud radiative kernels defined at the midpoints of the optical depth bins of the ISCCP simulator and log-linearly interpolate them to scaled optical depths defined according to Eq. (12) of Li et al. (2005). Applying this scaling reduced the slope shown in Fig. 3f from 1.43 to 0.97, significantly improving the agreement between the SW cloud feedback calculated with the cloud radiative kernel and that calculated by adjusting the change in SWCF.

In the LW, a different scaling was applied in the radiative transfer code of the AGCM4.0 model. Although the code does take into account the effect of horizontal variability in cloud fields on LW radiative transfer, it is not a simple modification of the optical thickness since the inhomogeneity was developed right into the radiative transfer solution (J. Cole, personal communication, 2011). Nevertheless, we scale the LW cloud radiative kernel in the same manner as the SW radiative kernel. This modestly improved the agreement between the cloud radiative kernel and adjusted change in LW cloud forcing-computed feedbacks, with the slope shown in Fig. 3f decreasing from 1.25 to 1.14.

APPENDIX B

Sensitivity Studies

Cloud feedbacks computed using cloud radiative kernels are sensitive to a number of assumptions made

in the construction of the kernels and in their implementation across models. Here we quantify the sensitivity of global mean cloud feedback estimates to several of these assumptions to better understand the uncertainties in our method.

a. Sensitivity of feedback estimates to the temperature and humidity profile used as input to the Fu–Liou radiation code

We have assessed this sensitivity by recalculating the kernels six times, each time using one of the six models' temperature and humidity profiles as input to the radiation code. These kernels vary slightly from each other (primarily in the LW) because of the slight differences in the models' temperature structures. However, these variations have very little effect on the global mean cloud feedback estimates; averaged across the 11 models, the range (max minus min) of possible values of LW cloud feedback computed using kernels derived using 6 different models' temperature and humidity profiles is $0.029 \text{ W m}^{-2} \text{ K}^{-1}$, with no model's range exceeding $0.039 \text{ W m}^{-2} \text{ K}^{-1}$. In the SW, the average range is $0.005 \text{ W m}^{-2} \text{ K}^{-1}$, with no model's range exceeding $0.006 \text{ W m}^{-2} \text{ K}^{-1}$.

b. Sensitivity of feedback estimates to the finite bin size of the ISCCP simulator histogram

The finite bin size of the ISCCP simulator histogram causes two main sources of uncertainty. The first, to which we can assess the sensitivity of our results, is uncertainty in the cloud radiative kernel calculation due to the choice of representative cloud properties for each bin. If the cloud distribution within a bin is skewed such that its properties are different from those at the CTP and τ midpoints, then a kernel generated assuming cloud properties of the midpoints will yield a less accurate estimate of the feedback than a kernel generated assuming more representative cloud properties.

In Table A1 we attempt to quantify the uncertainty in kernel-calculated feedbacks due to uncertainty in the representative cloud properties of each bin used to generate the kernels. In the "Standard" column are feedbacks computed using the standard kernel calculation in which TOA fluxes computed for clouds having properties determined by the four corners of each bin of the histogram are averaged together to compute one kernel value for each bin. The "min" and "max" columns represent the minimum and maximum of the four possible cloud feedbacks computed using the kernels corresponding to cloud properties defined at the corners of each bin (i.e., small τ and CTP, large τ and CTP, small τ and large CTP, and large τ and small CTP). Clearly, both LW

and SW cloud feedback estimates depend sensitively on which within-bin cloud properties are chosen when generating the kernel. For both LW and SW cloud feedbacks, the biggest difference in magnitudes are between those calculated with kernels defined at the thin, low corner and at the thick, high corner (not shown). LW cloud feedback estimates range by $0.17 \text{ W m}^{-2} \text{ K}^{-1}$, on average, and tend to be more sensitive to whether the minimum or maximum of each CTP bin edge is used (not shown). SW cloud feedback estimates range by $0.23 \text{ W m}^{-2} \text{ K}^{-1}$, on average, and tend to be more sensitive to whether the minimum or maximum of each τ bin is used (not shown). It is highly unlikely that the radiative properties of a cloud whose CTP and τ correspond to the corner of a bin are representative of the average radiative properties of clouds located within that bin. Thus, we consider the extrema of global mean cloud feedback estimates provided in Table A1 to be very conservative bounds on the true cloud feedback. Note that this feature of the radiative kernel technique only arises because the kernels are matched to the broad bins of the ISCCP simulator. Kernels generated to match higher-resolution cloud fraction histograms (like in Zelinka and Hartmann 2011) will be less prone to such uncertainties.

The second source of uncertainty arising from the finite bin size is the inability to capture within-bin changes in clouds that impact radiation. This is because cloud fraction within a given bin of the histogram can stay constant while the optical depth and vertical distribution of clouds within that bin changes. For example, a hypothetical distribution of clouds with optical depth 4 located at 300 hPa that shift to an optical depth of 8 at 200 hPa remain within the same CTP– τ classification. Since this would not appear as a cloud fraction change, its impact on radiation would not be recorded using the cloud radiative kernel technique. Although we cannot quantify the sensitivity to this issue with the available data, we note that cloud changes are coherent across bins such that shifts occurring within bins are manifested in the broader cloud distribution. As shown in Ockert-Bell and Hartmann (1992), covariance between different cloud types means that greater than 80% of the fluctuations in both OLR and TOA albedo can be explained by considering only 5–7 representative cloud types. That such correlation exists between cloud fraction changes occurring among different cloud types makes it likely that subsampling their fraction in CTP- and τ -space can still capture the relevant changes. It is also unlikely that the good agreement between cloud feedbacks computed using our cloud radiative kernels and those computed using the adjusted change in cloud forcing method of Shell et al. (2008) and Soden et al.

(2008) would have resulted if within-bin cloud changes were radiatively dominant.

c. Sensitivity of intermodel spread in SW cloud feedback to differences in mean-state clear-sky surface albedo

Before using the cloud radiative kernels to compute cloud feedback, they are mapped by linear interpolation from their native latitude–albedo space to latitude–longitude space using the clear-sky surface albedo at each location and month in the control climate. This feature of the kernel technique implies that some of the intermodel spread in SW cloud feedback will arise simply from differences in control climate clear-sky surface albedo across models. To assess this effect, we computed hypothetical SW feedbacks in each model by mapping the SW cloud radiative kernels to clear-sky albedos from different models' control climates. In each case, the cloud changes were the same as in the correct calculation, but the underlying albedo was taken from a different model. Within a given model, the hypothetical SW cloud feedbacks computed using other models' control climate surface albedos deviate from the true feedback by not more than $0.05 \text{ W m}^{-2} \text{ K}^{-1}$ on average. The range of SW cloud feedbacks across the 11-model ensemble, which is $1.11 \text{ W m}^{-2} \text{ K}^{-1}$ for the base calculation, varies only slightly from if only one model's control climate clear-sky surface albedo is used in all calculations. The end-members are the calculations using only the IPSL CM4 and HadSM3 models' albedo fields, for which the intermodel spread becomes 1.03 and $1.13 \text{ W m}^{-2} \text{ K}^{-1}$, respectively. Using all possible combinations of cloud changes and mean-state albedos, the intermodel spread ranges from 1.03 to $1.16 \text{ W m}^{-2} \text{ K}^{-1}$. Clearly the intermodel spread in control climate clear-sky surface albedo has a small impact on the intermodel spread in SW cloud feedback.

d. Sensitivity of feedback estimates to the restriction of the technique to sunlit points

Simulated cloud fields are only present for sunlit months in which a passive satellite sensor would retrieve visible optical depths (and are undefined otherwise). Only the sunlit portion of the diurnal cycle of cloudiness is sampled by the ISCCP simulator, and in polar regions, entire months are devoid of cloud information when the sun does not rise above the horizon. This is potentially problematic for diagnosing LW cloud feedback because cloud fields impact LW radiation at all times, not just when the sun is up. Thus, if the change in cloud properties between the $2 \times \text{CO}_2$ climate and the $1 \times \text{CO}_2$ climate is systematically different between

night and day or between dark and sunlit seasons, this technique will be biased, capturing only the cloud changes that occur for sunlit months. We find that in the annual mean, the adjusted change in LW cloud forcing at high latitudes agrees to within $0.1 \text{ W m}^{-2} \text{ K}^{-1}$ of the value computed when only sunlit months are sampled, suggesting that this is not a major issue. Cloud changes occurring when the sun is down do not impact SW radiative fluxes; however, because the simulator-derived cloud fraction at these locations and months is undefined, we artificially set the SW cloud feedback to zero. This ensures that a correct annual mean SW cloud feedback is computed (i.e., it includes zeros and is therefore not biased toward larger magnitudes). Thus the restriction of simulator application to sunlit months has no effect on SW cloud feedback estimates.

REFERENCES

- Ackerman, T. P., K. N. Liou, F. P. J. Valero, and L. Pfister, 1988: Heating rates in tropical anvils. *J. Atmos. Sci.*, **45**, 1606–1623.
- Allan, R. P., 2011: Combining satellite data and models to estimate cloud radiative effect at the surface and in the atmosphere. *Meteor. Appl.*, **18**, 324–333.
- Bony, S., and J. L. Dufresne, 2005: Marine boundary layer clouds at the heart of tropical cloud feedback uncertainties in climate models. *Geophys. Res. Lett.*, **32**, L20806, doi:10.1029/2005GL023851.
- , —, H. L. Treut, J. J. Morcrette, and C. Senior, 2004: On dynamic and thermodynamic components of cloud changes. *Climate Dyn.*, **22**, 71–68.
- Cess, R. D., and Coauthors, 1990: Intercomparison and interpretation of cloud-climate feedback processes in nineteen atmospheric general circulation models. *J. Geophys. Res.*, **95** (D10), 16 601–16 615.
- Charlock, T. P., and V. Ramanathan, 1985: The albedo field and cloud radiative forcing produced by a general circulation model with internally generated cloud optics. *J. Atmos. Sci.*, **42**, 1408–1429.
- Fu, Q., 1996: An accurate parameterization of the solar radiative properties of cirrus clouds for climate models. *J. Climate*, **9**, 2058–2082.
- , and K. N. Liou, 1992: On the correlated k -distribution method for radiative transfer in nonhomogeneous atmospheres. *J. Atmos. Sci.*, **49**, 2139–2156.
- Gregory, J., and M. Webb, 2008: Tropospheric adjustment induces a cloud component in CO_2 forcing. *J. Climate*, **21**, 58–71.
- Hannay, C., D. L. Williamson, J. J. Hack, J. T. Kiehl, J. G. Olson, S. A. Klein, C. S. Bretherton, and M. Kohler, 2009: Evaluation of forecasted southeast pacific stratocumulus in the NCAR, GFDL, and ECMWF models. *J. Climate*, **22**, 2871–2889.
- Hartmann, D. L., L. A. Moy, and Q. Fu, 2001: Tropical convection and the energy balance at the top of the atmosphere. *J. Climate*, **14**, 4495–4511.
- Jin, Y., and W. B. Rossow, 1997: Detection of cirrus overlapping low-level clouds. *J. Geophys. Res.*, **102**, 1727–1737.
- Klein, S. A., and C. Jakob, 1999: Validation and sensitivities of frontal clouds simulated by the ECMWF model. *Mon. Wea. Rev.*, **127**, 2514–2531.

- Kubar, T. L., D. L. Hartmann, and R. Wood, 2007: Radiative and convective driving of tropical high clouds. *J. Climate*, **20**, 5510–5526.
- Li, J., 2000: Accounting for overlap of fractional cloud in infrared radiation. *Quart. J. Roy. Meteor. Soc.*, **126**, 3325–3342.
- , and H. W. Barker, 2002: Accounting for unresolved clouds in a 1D infrared radiative transfer model. Part II: Horizontal variability of cloud water path. *J. Atmos. Sci.*, **59**, 3321–3339.
- , S. Dobbie, P. Risnen, and Q. Min, 2005: Accounting for unresolved clouds in a 1-D solar radiative-transfer model. *Quart. J. Roy. Meteor. Soc.*, **131**, 1607–1629.
- McAvaney, B. J., and H. Le Treut, 2003: The cloud feedback intercomparison project: (CFMIP). *CLIVAR Exchanges*, No. 26 (Suppl. Contributions), International CLIVAR Project Office, Southampton, United Kingdom, 1–4.
- Ockert-Bell, M. E., and D. L. Hartmann, 1992: The effect of cloud type on earth's energy balance: Results for selected regions. *J. Climate*, **5**, 1157–1171.
- Ringer, M. A., and Coauthors, 2006: Global mean cloud feedbacks in idealized climate change experiments. *Geophys. Res. Lett.*, **33**, L07718, doi:10.1029/2005GL025370.
- Rossow, W. B., and R. A. Schiffer, 1999: Advances in understanding clouds from ISCCP. *Bull. Amer. Meteor. Soc.*, **80**, 2261–2287.
- Shell, K. M., J. T. Kiehl, and C. A. Shields, 2008: Using the radiative kernel technique to calculate climate feedbacks in NCAR's Community Atmospheric Model. *J. Climate*, **21**, 2269–2282.
- Slingo, A., 1989: A GCM parameterization for the shortwave radiative properties of water clouds. *J. Atmos. Sci.*, **46**, 1419–1427.
- Soden, B. J., and I. M. Held, 2006: An assessment of climate feedbacks in coupled ocean–atmosphere models. *J. Climate*, **19**, 3354–3360.
- , A. J. Broccoli, and R. S. Hemler, 2004: On the use of cloud forcing to estimate cloud feedback. *J. Climate*, **17**, 3661–3665.
- , I. M. Held, R. Colman, K. M. Shell, J. T. Kiehl, and C. A. Shields, 2008: Quantifying climate feedbacks using radiative kernels. *J. Climate*, **21**, 3504–3520.
- Stubenrauch, C. J., W. B. Rossow, F. Chéruiy, A. Chédin, and N. A. Scott, 1999: Clouds as seen by satellite sounders (3I) and imagers (ISCCP). Part I: Evaluation of cloud parameters. *J. Climate*, **12**, 2189–2213.
- Tsushima, Y., and Coauthors, 2006: Importance of the mixed-phase cloud distribution in the control climate for assessing the response of clouds to carbon dioxide increase: A multi-model study. *Climate Dyn.*, **27**, 113–126.
- Webb, M., C. Senior, S. Bony, and J. J. Morcrette, 2001: Combining ERBE and ISCCP data to assess clouds in the Hadley Centre, ECMWF and LMD atmospheric climate models. *Climate Dyn.*, **17**, 905–922.
- , and Coauthors, 2006: On the contribution of local feedback mechanisms to the range of climate sensitivity in two GCM ensembles. *Climate Dyn.*, **27**, 17–38.
- Wetherald, R. T., and S. Manabe, 1980: Cloud cover and climate sensitivity. *J. Atmos. Sci.*, **37**, 1485–1510.
- Williams, K., and G. Tselioudis, 2007: GCM intercomparison of global cloud regimes: Present-day evaluation and climate change response. *Climate Dyn.*, **29**, 231–250.
- , and M. Webb, 2009: A quantitative performance assessment of cloud regimes in climate models. *Climate Dyn.*, **33**, 141–157.
- Wyant, M. C., C. S. Bretherton, J. T. Bacmeister, J. T. Kiehl, I. M. Held, M. Zhao, S. A. Klein, and B. J. Soden, 2006: A comparison of low-latitude cloud properties and responses in AGCMs sorted into regimes using mid-tropospheric vertical velocity. *Climate Dyn.*, **27**, 261–279.
- Yokohata, T., M. J. Webb, M. Collins, K. D. Williams, M. Yoshimori, J. C. Hargreaves, and J. D. Annan, 2010: Structural similarities and differences in climate responses to CO₂ increase between two perturbed physics ensembles. *J. Climate*, **23**, 1392–1410.
- Zelinka, M. D., and D. L. Hartmann, 2011: The observed sensitivity of high clouds to mean surface temperature anomalies in the tropics. *J. Geophys. Res.*, **116**, D23103, doi:10.1029/2011JD016459.
- , S. A. Klein, and D. L. Hartmann, 2012: Computing and partitioning cloud feedbacks using cloud property histograms. Part II: Attribution to Changes in Cloud Amount, Altitude, and Optical Depth. *J. Climate*, **25**, 3736–3754.